Photopyroelectric thin-film instrumentation and impulse-response detection. Part I: A theoretical model

Joan F. Power and Andreas Mandelis

Photoacoustic and Photothermal Sciences Laboratory, Department of Mechanical Engineering, University of Toronto, Toronto, Ontario M5S 1A4, Canada

(Received 7 May 1987; accepted for publication 21 July 1987)

Thin-film pyroelectric effect detectors provide a simple means of measuring thermal properties of solid samples. The present work reports a time-delay theoretical model of thin-film pyroelectric detection which enables the recovery of thermal diffusivity and thermal conductivity information from the impulse response of the pyroelectric system.

INTRODUCTION

The photopyroelectric (P^2E) effect has provided a recent method of transient thermometry and calorimetry, in which a voltage or current is produced in a contact thin-film pyroelectric sensor as the result of heat conduction through a sample layer on the surface of the film.[1,2] The voltage or current change results from a temperature change in the pyroelectric material, which induces polarization changes. Many materials which are piezoelectric also exhibit pyroelectricity: for this reason pyroelectric elements have been traditionally fabricated from piezoelectrics.[2] More recently, thin-film pyroelectric materials have emerged. These are low-cost, highly versatile, fast-rise-time elements. Samples of interest may be coated or deposited directly on the pyroelectric film, and studied essentially *in situ*.

The components of a typical thin-film photopyroelectric detector consist of a sample, in contact with the pyroelectric film, which is itself supported by a backing layer (Fig. 1). Recent theories of photopyroelectric signal detection[3,4] have been developed in the frequency domain, for this model. Frequency-domain responses have traditionally been studied because the measurements may be readily made with lock-in amplifiers. Pulsed experiments, on the other hand, directly yield a visualization of the transit times of thermal signals through the sample, which is not readily available from time-multiplexed frequency-domain representations. However, past theoretical treatments of pulsed photopyroelectric signal generation have not taken into account the finite thickness of the film and the properties of the backing material. A theoretical treatment which assumes a semi-infinite pyroelectric element is valid for measurements which use thick substrates such as PZT's for detection: a more detailed theory is required for time-domain pyroelectric detection using thin films. In this work we present such a theory which can satisfactorily account for the response of fast rise-time thin-film pyroelectric detectors later used with our impulse-response photopyroelectric instrumentation.

I. THE MODEL

The mechanism of signal generation in pyroelectrics, in general, is the production of net polarization changes across the bulk of the pyroelectric as the result of induced temperature changes.[2,5] The change in polarization with temperature gives rise to a voltage V given by

$$V(t) = (pd/\varepsilon)\langle \Delta T(x,t)\rangle, \tag{1}$$

where d is the thickness of the pyroelectric element, ε is the dielectric constant of the pyroelectric, and $\langle \Delta T(x,t)\rangle$ is the spatially averaged temperature in the material. The parameter p is the pyroelectric coefficient of the device which is a figure of merit, giving the extent of polarization change of the pyroelectric per unit temperature change.

The spatially averaged temperature change in the pyroelectric is given, by definition, as[2]

$$\langle \Delta T(x,t)\rangle = \frac{1}{d}\int_{-(l+d)}^{-l} T_3(x,t)\,dx\,, \tag{2}$$

where l is the sample thickness and $T_3(x,t)$ is the temperature profile in the film layer [layer (iii), see Fig. 1].

The temperature distribution in the pyroelectric, for a unit heat impulse, is available from a one-dimensional Green's function treatment of heat conduction in a four-layer system. The treatment is similar to theories developed by Mandelis *et al.*[6] and Yeack *et al.*[7]

In Fig. 1, the heat conduction equation is solved for each of layers (i)–(iv), assuming excitation of the sample with a unit impulse heat source at $x = x'$ and $t = t'$:

$$\text{gas:}\quad \frac{\partial^2 T_1}{\partial x^2} - \frac{1}{\alpha_1}\frac{\partial T_1}{\partial t} = 0, \tag{3}$$

$$\text{sample:}\quad \frac{\partial^2 T_2}{\partial x^2} - \frac{1}{\alpha_2}\frac{\partial T_2}{\partial t} = -\delta(x-x')\delta(t-t')\,, \tag{4}$$

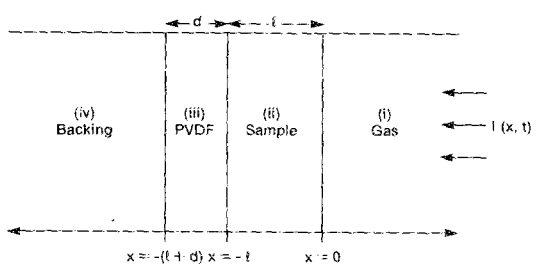

FIG. 1. Schematic of the four-layer theoretical model for the sample/pyroelectric system.

 0034-6748/87/112018-06$01.30

pyroelectric thin film: $$\frac{\partial^2 T_3}{\partial x^2} - \frac{1}{\alpha_3}\frac{\partial T_3}{\partial t} = 0, \quad (5)$$

backing: $$\frac{\partial^2 T_4}{\partial x^2} - \frac{1}{\alpha_4}\frac{\partial T_4}{\partial t} = 0, \quad (6)$$

where α_i is the thermal diffusivity of the ith layer.

Laplace transformation of these equations with respect to time gives homogeneous solutions, with respect to x, of the form

$$\overline{T}_i(x,s) = A_1(s)e^{-q_i x} + A_2(s)e^{q_i x}. \quad (7)$$

The coefficients A_1 and A_2 depend on the boundary conditions, and q_i contains the Laplace domain variable s in the form

$$q_i = (s/\alpha_i)^{1/2}.$$

The inhomogeneous solution in region (ii) for $t' = 0$ is given by the source Green's function[8,9]

$$T_{2(I)}(x,t) = (1/2\sqrt{\alpha_2 \pi t})e^{-(x-x')^2/4\alpha_2 t}, \quad (8)$$

where x' is the spatial location of the Dirac source $\delta(x-x')$.

The Laplace transform of Eq. (8) is

$$\overline{T}_{2(I)}(x,s) = (1/2\alpha_2 q_2)e^{-q_2|x-x'|}. \quad (9)$$

The temperature distributions in regions (i)–(iv) are then written as

(i) $$\overline{T}_1(x,s) = A_1 e^{-q_1 x} \quad (x>0), \quad (10)$$

(ii) $$\overline{T}_2(x,s) = A_2 e^{q_2 x} + A_3 e^{-q_2 x} + (1/2\alpha_2 q_2) \times e^{-q_2|x-x'|} \quad (-l \leqslant x \leqslant 0), \quad (11)$$

(iii) $$\overline{T}_3(x,s) = A_4 e^{q_3(x+l)} + A_5 e^{-q_3(x+l)} \quad [-(l+d) \leqslant x \leqslant -l], \quad (12)$$

(iv) $$\overline{T}_4(x,s) = A_6 e^{q_4[x+(l+d)]} \quad [x \leqslant -(l+d)]. \quad (13)$$

The coefficients A_1–A_6 in Eqs. (10)–(13) are determined simultaneously, assuming continuity of heat flux and temperature at the boundaries. Furthermore, if the location of the heat source is at the sample/gas interface then $x' = 0$. In that case, the Laplace transform of the temperature distribution in the pyroelectric film is given by

$$\begin{aligned}\overline{T}_3(x,s) = {} & [2(b_{43}+1)e^{q_3(x+l+d)} - 2(b_{43}-1)e^{-q_3(x+l+d)}] \\ & \times \{\alpha_2 q_2 \{(b_{43}-1)e^{-q_3 d}[(b_{32}-1)(b_{12}+1)e^{q_2 l} + (b_{32}+1)(b_{12}-1)e^{-q_2 l}] \\ & + (b_{43}+1)e^{q_3 d}[(b_{32}+1)(b_{12}+1)e^{q_2 l} - (b_{12}-1)(b_{32}-1)e^{-q_2 l}]\}\}^{-1}, \end{aligned} \quad (14)$$

where the thermal transport coefficients b_{ij} are defined as $b_{ij} = k_i \alpha_j^{1/2}/k_j \alpha_i^{1/2}$, i and j being adjacent layers in the model of Fig. 1.

The denominator may be expanded and expressed in the form

$$\alpha_2 q_2 (b_{43}+1)(b_{12}+1)(b_{32}+1)e^{q_3 d}e^{q_2 l}(1+\xi),$$

where

$$\xi = \gamma_1\gamma_2 e^{-2q_3 d} + \gamma_1\gamma_3 e^{-2q_1 d - 2q_2 l} - \gamma_2\gamma_3 e^{-2q_2 l}, \quad (15)$$

and

$$\gamma_1 = \frac{(b_{43}-1)}{(b_{43}+1)}, \quad \gamma_2 = \frac{(b_{32}-1)}{(b_{32}+1)}, \quad \gamma_3 = \frac{(b_{12}-1)}{(b_{12}+1)}.$$

The factor $1/(1+\xi)$ may be expressed in a Taylor series to give an expression of the form

$$\overline{T}(x,s) = \frac{[2(b_{43}+1)e^{q_3(x+l)-q_2 l} - 2(b_{43}-1)e^{-q_3(x+l+2d)-q_2 l}]}{\alpha_2 q_2 (b_{43}+1)(b_{12}+1)(b_{32}+1)} \sum_{n=0}^{\infty}(-1)^n \xi^n. \quad (16)$$

Equation (16) forms the nucleus of our theoretical four-layer treatment. Instead of inverting (16) directly, it is more informative to consider a number of realistic experimental approximations which apply generally in measurements on solid samples with thin-film detectors such as polyvinylidene difluoride (PVDF). These situations are discussed in the next section.

II. EXPERIMENTAL CONDITIONS AND APPROXIMATIONS TO THE MODEL

To a first approximation, the relative values of the transport coefficients, b_{ij}, determine the shape of the time delay domain profile and the relative importance of heat conduction processes in the backing, gas, and sample layers.

For materials studies, the gas layer is typically air, while the sample is a solid. For a gas/solid interface, there is a large mismatch in thermal properties, with $b_{12} \ll 1$ regardless of whether the sample is a good thermal conductor or an insulator. For the film/backing interface, the choice of a metallic backing such as stainless steel easily ensures that $b_{43} \gg 1$. This is true for metal backings in general. If air is used as the backing material we have the condition $b_{43} \ll 1$. The use of solid insulating materials such as vulcanized rubber gives $b_{43} \approx 1$ with the consequence that there is no discontinuity between the thermal properties of the film and the backing.

We next proceed to derive the expression for the average temperature profile in the film, for several experimentally important cases.

Case 1: Semi-infinite pyroelectric or continuous thermal properties of backing/pyroelectric

If the assumptions are made that $b_{12} \ll 1$ and $b_{43} = 1$ in Eq. (16), we are dealing with a situation in which there is no

heat conduction in the gas layer and that the detector is semi-infinite thermally. These conditions match the assumption of an earlier time domain theory reported for a semi-infinite pyroelectric.[7] In that case, the resulting equation is

$$\overline{T}_3(x,s)=\frac{2e^{q_3(x+l)-q_2l}}{\alpha_2 q_2(b_{32}+1)}\sum_{n=0}^{\infty}(-1)^n\frac{(b_{32}-1)^n}{(b_{32}+1)^n}e^{-2q_2nl}. \tag{17}$$

If we assume that $d\to\infty$, integration of Eq. (17) over the film thickness followed by inverse Laplace transformation gives the equation derived in earlier work[7]:

$$\langle T_3(x,t)\rangle=\frac{2(\alpha_2\alpha_3)^{1/2}}{\alpha_2(b_{32}+1)}\times\sum_{n=0}^{\infty}\left(\frac{1-b_{32}}{1+b_{32}}\right)^n\operatorname{erfc}\left(\frac{(2n+1)l}{2\alpha_2^{1/2}t^{1/2}}\right). \tag{18}$$

If the film thickness is finite, the resulting expression is

$$\langle T_d(x,t)\rangle=(-1)\frac{2(\alpha_2\alpha_3)^{1/2}}{\alpha_2(b_{32}+1)}\sum_{n=0}^{\infty}(-1)^n\gamma^n\times\left[\operatorname{erfc}\left(\frac{(2n+1)l}{2\sqrt{\alpha_2 t}}+\frac{d}{2\sqrt{\alpha_3 t}}\right)-\operatorname{erfc}\left(\frac{(2n+1)l}{2\sqrt{\alpha_2 t}}\right)\right]. \tag{19}$$

Case 2a: Metallic backing ($b_{43}\gg 1$). Large thermal mismatch at $x=0(b_{12}\ll 1)$. Thermally thick samples

With the conditions $b_{43}\gg 1$ and $b_{12}\ll 1$, Eq. (16) becomes

$$\overline{T}_3(x,s)=\frac{2(e^{q_3(x+l)-q_2l}-e^{-q_3(x+l+2d)-q_2l})}{\alpha_2 q_2(b_{32}+1)}\times\sum_{n=0}^{\infty}(-1)^n\xi^n, \tag{20}$$

where $\xi=\gamma_2(e^{-2q_3d}+e^{-2q_2l})-e^{-2(q_3d+q_2l)}$.

For the case of a thermally thick sample, we have the condition $2q_2l\gg 2q_3d$. Keeping in mind that $s\leftrightarrow 2\pi j/\tau$, where $j=\sqrt{-1}$ and τ is the time-delay-domain variable, one can directly verify the condition $q_2l\gg q_3d$ in the thermally thick regime. Accordingly,

$$\xi^n=[(b_{32}-1)/(b_{32}+1)]^n e^{-2q_3nd}.$$

Termwise integration of Eq. (20) over the film thickness, followed by inverse Laplace transformation gives

$$\langle T_3(x,t)\rangle=\frac{2(\alpha_2\alpha_3)^{1/2}}{\alpha_2(b_{32}+1)}\sum_{n=0}^{\infty}\gamma_2^n(-1)^n\times\left(\operatorname{erfc}\sqrt{\frac{\tau_{1n}}{4t}}-2\operatorname{erfc}\sqrt{\frac{\tau_{2n}}{4t}}+\operatorname{erfc}\sqrt{\frac{\tau_{3n}}{4t}}\right), \tag{21}$$

where

$$\tau_{1n}^{1/2}=\frac{2nd}{\alpha_3^{1/2}}+\frac{l}{\alpha_2^{1/2}},\quad \tau_{2n}^{1/2}=\frac{(2n+1)d}{\alpha_3^{1/2}}+\frac{l}{\alpha_2^{1/2}},$$

and

$$\tau_{3n}^{1/2}=\frac{2(n+1)d}{\alpha_3^{1/2}}+\frac{l}{\alpha_2^{1/2}}.$$

Case 2b: Metallic backing ($b_{43}\gg 1$) with thermally thin sample and large thermal mismatch at $x=0(b_{12}\ll 1)$

The temperature profile's Laplace transform has the same form as Eq. (20) except that $q_2l\ll q_3d$. Therefore, $\xi\approx\gamma_2 e^{-2q_2l}$ and the resulting spatially averaged temperature temporal profile has the form identical to Eq. (21) except that

$$\tau_{1n}^{1/2}=\frac{(2n+1)l}{\alpha_2^{1/2}},\quad \tau_{2n}^{1/2}=\frac{(2n+1)l}{\alpha_2^{1/2}}+\frac{d}{\alpha_3^{1/2}},\quad \tau_{3n}^{1/2}=\frac{2d}{\alpha_3^{1/2}}+\frac{(2n+1)l}{\alpha_3^{1/2}}. \tag{22}$$

General discussion: Results of the theory

The exact form of the signal extracted from a pyroelectric measurement depends on whether the current or voltage response of the thin-film element is recovered. The voltage response of the P^{2}E detector has a form which is directly proportional to the average temperature profile in the thin film, as given by Eq. (1). For the pyroelectric detector under load, Eq. (1) is differentiated to give

$$I(t)=\frac{pd}{\varepsilon}\frac{\partial\langle\Delta T(x,t)\rangle}{\partial t}. \tag{23}$$

It is this form of the pyroelectric response with which the present work mainly concerns itself, since it corresponds to the conditions of our experimental investigation made in Parts II and III below.[10,11] In addition, we concentrate on the consequences of the theory for thermally thick samples (case 2a) since this situation has been investigated in detail in Parts II and III of this work.

The basic character of the P^{2}E current response is best illustrated from case 2a presented in Eq. (19). Figure 2 compares the voltage and current-impulse responses for the case of a pyroelectric detector of finite thickness d supported by a backing with thermal properties indistinguishable from the pyroelectric. A sample with $l=500\,\mu$m and $\alpha_2=4.0\times10^{-7}$ m^2/s is contacted to the film. The voltage response in this case is obtained from Eq. (19), since $V(t)\propto\langle T_3(x,t)\rangle$.

The current response can be obtained directly from Eq. (19) upon time differentiation

$$I(t)=\frac{2k(\alpha_2\alpha_3)^{1/2}}{\alpha_2(b_{32}+1)}\frac{1}{8\sqrt{\pi}t^{3/2}}\times\sum_{n=0}^{\infty}(-1)^{n+1}\gamma_2^n\left(\tau_{1n}^{1/2}e^{-\tau_{1n}/4t}-\tau_{2n}^{1/2}e^{-\tau_{2n}/4t}\right), \tag{24}$$

where

$$\tau_{1n}^{1/2}=\frac{(2n+1)l}{\alpha_2^{1/2}},\quad \tau_{2n}^{1/2}=\frac{(2n+1)l}{\alpha_2^{1/2}}+\frac{d}{\alpha_3^{1/2}}.$$

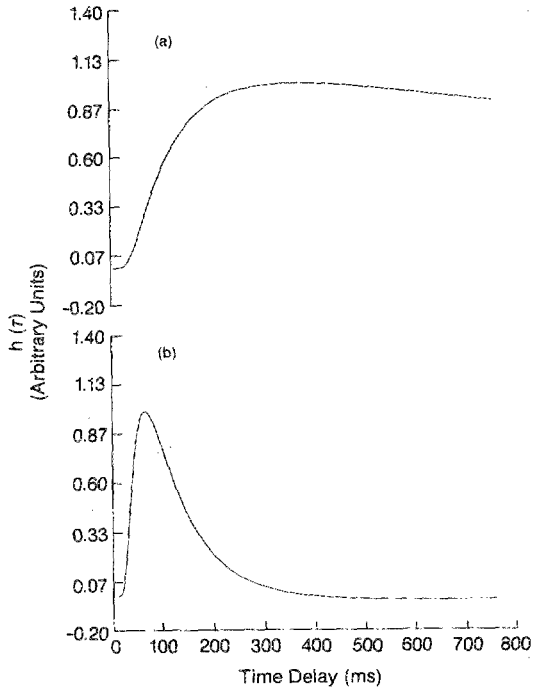

FIG. 2. (a) Voltage-impulse response and (b) current-impulse response. $\alpha_2 = 4.0\times10^{-7}$ m^2/s, the film thickness d is assumed to be 28 μm with $\alpha_3 = 6\times10^{-8}$ m^2/s (Ref. 5). Theoretical responses obtained from Eqs. (19) and (24) with the $n = 0$ term retained only.

The features of the voltage response [Fig. 2(a)] show a relatively sharp growth profile followed by a very slow decay. The decay of $V(t)$ takes place on a time scale exceeding hundreds of milliseconds and is generally so broad that it contains relatively little useful information. Thermal diffusivity information is recovered from the time delay of the voltage peak. The current response, on the other hand, depends on the time rate of change of the temperature in the pyroelectric rather than the temperature field itself. The peak of the current response thus corresponds to the inflection point of the temperature rise in the pyroelectric. The current response shows a decay past the maximum, with a drop in signal below the base line to a slightly negative value. The point at which the current response crosses the base line $[I(t) = 0]$ gives the time delay of the voltage-response maximum, since at this point, we have the condition $\partial V/\partial t = 0$ [see Eq. (23)]. The slightly negative value of the current response corresponds to the regime in which the voltage response begins to decay. The current response, then, in effect, is more sensitive to the information contained in the rising edge of the voltage-response curve, and yields a peak delay which is nearly four times earlier than the voltage-response maximum. It is important to extract an early time measurement of the sample thermal properties because of the contribution of three-dimensional heat conduction processes that could occur at very late times, as well as the increasing contributions of $1/f$ noise in the measurement system.

Three-dimensional heat flow effects are expected to contribute at the lowest frequencies, for which the sample radius approaches the time-dependent thermal diffusion length in the sample.[12,13] For sample radii in the range 1–5 mm, which is typical for materials studies, three-dimensional heat conduction is not expected to make an important contribution at modulation frequencies above 1 Hz for glasses and other insulating materials, for which the condition $q_3 d \gg q_2 l$ applies.

Because it is a differential measurement, the current response is an inherently more sensitive indicator of transient heat conduction phenomena occurring in the sample than the voltage response. Trends in the current response are intuitively obtainable from the voltage response. Conditions which delay the voltage-response peak, increase the peak width and peak delay of current response. As the voltage rise-time profile becomes very broad, the current-response peak tails off very slowly in time.

The next step is to consider the effects of adding a backing to the film, with different thermal properties. The pyroelectric current response, for case 2a is given by

$$I(t) = \frac{kA}{t^{3/2}} \sum_{n=0}^{\infty} (-1)^{n+1}\gamma^n \times \left(\tau_{1n}^{1/2} e^{-\tau_{1n}/4t} - 2\tau_{2n}^{1/2} e^{-\tau_{2n}/4t} + \tau_{3n}^{1/2} e^{-\tau_{3n}/4t}\right), \quad (25)$$

with τ_{1n}, τ_{2n}, τ_{3n} given by Eq. (21). A is a constant, incorporating the static thermal properties of the sample/pyroelectric. In the case of a metal backing, with $b_{43} \gg 1$, we arrive at the physical situation of having attached a heat sink to the back surface of the pyroelectric (Fig. 3). The temperature gradient across the film is steeper in this case and the average temperature in the film is lower. This temperature gradient is determined by the heat flux arriving at the rear surface of the sample, and results in a faster rise time of the temperature field in the pyroelectric with a concommitant decrease in the peak delay and peak width of the current response of the pyroelectric than the case with a pyroelectric detector/sample interface of the same thermal properties ($b_{43} = 1$).

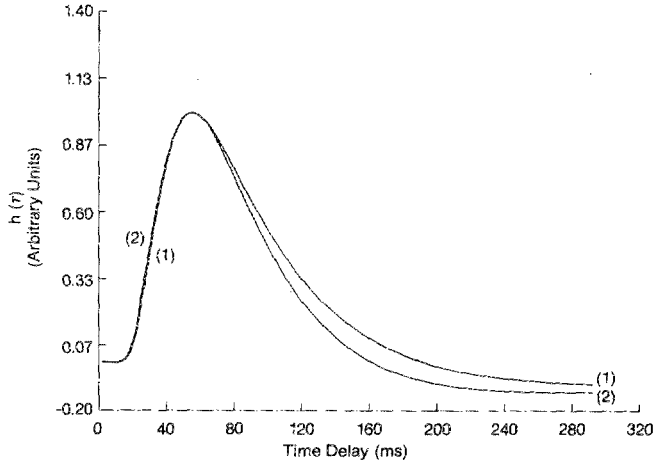

FIG. 3. Current-impulse response of a 500-μm sample with stainless-steel backing ($b_{43} \gg 1$). Upper curve (1): response for $d = 28$ μm and $\alpha_2 = 4.0\times10^{-7}$ m^2/s; lower curve (2): $d = 9$ μm and $\alpha_2 = 3.5\times10^{-7}$ m^2/s. Both responses were obtained from Eq. (24) with $\gamma_2 = 0.7$ and $n = 5$ terms.

Similar effects are observed as d^2/α_3 is decreased. Figure 3 shows the effect of varying thermal transit time through the film, d^2/α_3, in going from 28- to 9-μm film. The thinner film (9 μm) responds faster than the 28-μm film, since the thicker film requires a longer period of time to build up to a maximum average temperature. The current-impulse response then is broader, and a smaller α_2 is required to maintain the same peak delay time.

Because of the diffusive nature of thermal-wave propagation, the temperature distribution broadens with distance traveled in the sample. The same energy is distributed over a larger volume in the case of a thicker sample, with the result that the temperature/time response is broadened, the arrival of temperature changes is delayed, and the overall signal magnitude is decreased. Broadening of the temperature–time profile also results in a direct decrease in the value of the temperature–time derivative, so the acquired pyroelectric signal is further diminished (Fig. 4).

While the effect of increasing l directly diminishes the magnitude of the peak response, this quantity is also sensitive to such experimental factors as the intensity of the heat source at the sample surface, and the irradiation geometry. It is, thus, not a precisely controllable quantity in a practice. Consequently, we have normalized the impulse-response profiles, (except in Fig. 4) so that the maximum value of the impulse response is set to unity at the peak of the response. Thickness and thermal diffusivity information is readily available from the peak delay time τ_d, peak width $\Delta\tau_d$, and zero crossing point τ_0 of the pyroelectric-current response. Throughout this work (Parts I–III), we define the "peak width" $\Delta\tau_d$ as the time delay between the peak maximum at τ_d, and the half-intensity point of the *trailing edge* of the impulse response. Figure 5 shows the theoretical relationship between τ_d, $\Delta\tau_d$, and τ_0 vs l^2. All of these quantities are nearly linear with l^2 (R, the correlation coefficient, >0.999), with τ_d exhibiting entirely linear relation to l^2. While the intercept is nonzero, this is an extrapolated limit only, and is not valid, since the theoretical development is limited, in the present case, to thermally thick samples.

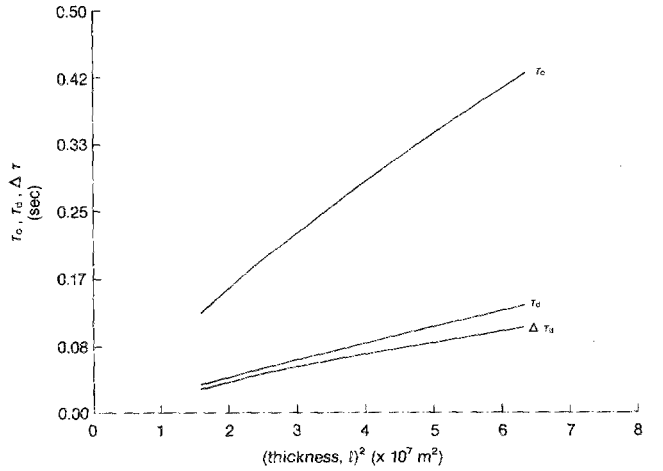

FIG. 5. Theoretical dependence of τ_0, τ_d, and $\Delta\tau_d$ on l^2. Results obtained from Eq. (24) with $\gamma_2 = 0.7$, $\alpha_2 = 4.0\times10^{-7}$ m^2/s, $d = 28\,\mu$m, and $n = 5$ terms in the series expansion.

A further important consequence of using thin-film pyroelectric detection is the effect of the thermal conductivity k_2 of the sample. An important factor which controls the decay time of the current response is the ratio γ_2. Large values of k_2 give relatively large values of γ_2, and vice versa. Figure 6 illustrates the effect of varying γ_2 from 0.1 (for an insulating solid sample) to 1.0 (typical of a metal sample) on the recovered current-impulse response. Similar trends were observed in earlier work.[7] Surprisingly, at first glance, the larger thermal conductivity gives the broader response. However, since large k_2 implies a very small b_{32}, physically, we have a large thermal mismatch at the detector/sample interface. Because of the very small k_3 for the pyroelectric, relative to k_2, the sample retains the thermal energy for a longer period because it is effectively reflected at the low-k interface presented by the pyroelectric. As b_{32} approaches unity, γ_2 approaches zero, and the sample pyroelectric inter-

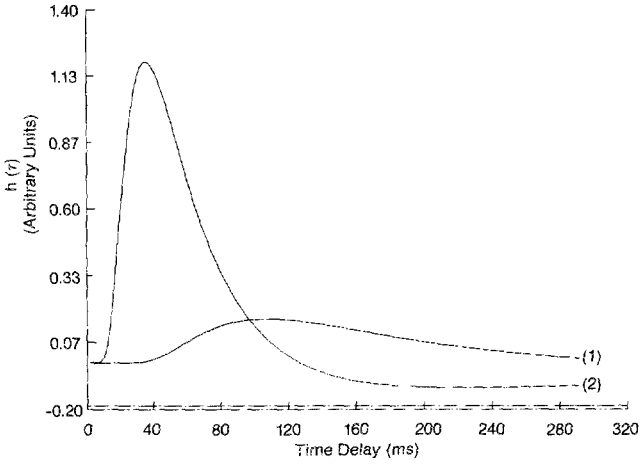

FIG. 4. Effect of sample thickness l on recovered impulse-response profile. Upper curve (1): $l = 700\,\mu$m; lower curve (2): $l = 400\,\mu$m. Responses were computed with Eq. (24) assuming $n = 5$ terms in series, and $\gamma_2 = 0.7$, $d = 28\,\mu$m, and $\alpha_2 = 4.0\times10^{-7}$ m^2/s.

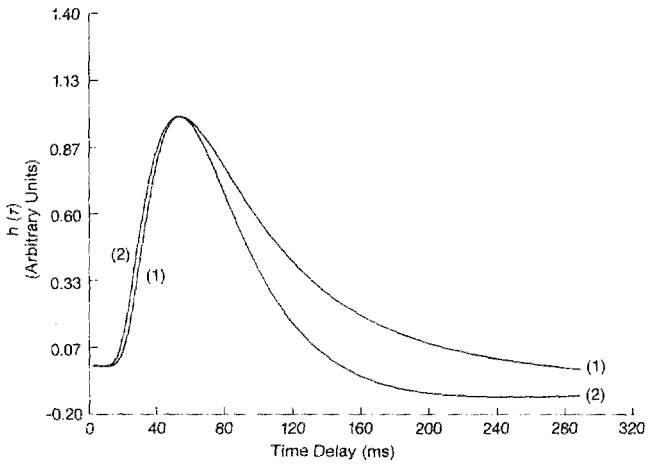

FIG. 6. Effect of γ_2 on recovered impulse response. Theoretical results obtained from Eq. (24) with $n = 5$ terms in series expansion; $d = 28\,\mu$m and $l = 500\,\mu$m. Upper curve (1): $\gamma_2 = 1.0$ and $\alpha_2 = 4.0\times10^{-7}$ m^2/s; lower curve (2): $\gamma_2 = 0.1$ and $\alpha_2 = 3.7\times10^{-7}$ m^2/s.

face properties become more or less continuous. Therefore, more of the energy propagating through the sample is communicated to the film per unit time, with the result that the pyroelectric response signal appears earlier and decays earlier (or equivalently, a *smaller* α_2 is required to yield the same peak delay). The response profiles predicted by our four-layer theory show greater sensitivity to changes in γ than the semi-infinite theory derived in earlier work.[7] This is due to the thinness of the film, which is more sensitive to thermal transport processes occurring in the sample layer. Because the film is thinner, the average temperature builds up much more quickly. Also, the heat sink on the rear surface of the sample ensures that the measurement is much more sensitive to processes occurring in the sample, which transmit or back-reflect thermal energy.

The consequences of this four-layer model for thermal diffusivity and film thickness measurements on relatively thick materials, are that both thermal diffusivity and thermal conductivity information are obtained from the pyroelectric current response. The peak delay time is relatively insensitive to variations in γ and, therefore, k_2, so that thermal diffusivity information is readily available to an error no more than 10%–15%. Samples may be fitted with a single thermal parameter to get a good initial estimate of α_2. Further refinement of the α_2 value, in combination with trial values of k_2, enable the fitting of the entire current/time response of the sample/pyroelectric system.

[1]A. C. Tam and H. Coufal, Appl. Phys. Lett. **42**, 33 (1983).
[2]H. Coufal, IEEE Trans. UFFC, **UFFC 33**, 507 (1986).
[3]A. Mandelis and M. M. Zver, J. Appl. Phys. **57**, 4421 (1985).
[4]P. K. John, L. C. M. Miranda, and A. C. Rastogi, Phys. Rev. B **34**, 4342 (1986).
[5]KYNAR™ Piezo Film Technical Manual, Pennwalt Corp., King of Prussia, PA, 1983.
[6]A. Mandelis, L. M. L. Borm, and J. Tiessinga, Rev. Sci. Instrum. **57**, 622 (1986).
[7]C. E. Yeack, R. L. Melcher, and S. S. Jha, J. Appl. Phys. **53**, 3947 (1982).
[8]H. S. Carslaw and J. C. Jaeger, in *Conduction of Heat in Solids*, 2nd ed. (Clarendon, Oxford, 1959), Chap. 14.
[9]P. M. Morse and H. Feshbach, in *Methods of Theoretical Physics* (McGraw-Hill, New York, 1953), Chap. 9, Vol. 1.
[10]J. F. Power and A. Mandelis, Part II, Rev. Sci. Instrum. **58**, 2024 (1987).
[11]J. F. Power and A. Mandelis, Part III, Rev. Sci. Instrum. **58**, 2033 (1987).
[12]R. S. Quimby and W. M. Yen, Appl. Phys. Lett. **35**, 43 (1979).
[13]H. C. Chow, J. Appl. Phys. **51**, 4053 (1980).